J Therm Anal Calorim (2011) 103:943–955
DOI 10.1007/s10973-010-1162-5

Thermal decomposition kinetics of potassium iodate

K. Muraleedharan · M. P. Kannan · T. Ganga Devi

Received: 20 September 2010 / Accepted: 3 November 2010 / Published online: 8 December 2010

Abstract The thermal decomposition of potassium iodate (KIO_3) has been studied by both non-isothermal and isothermal thermogravimetry (TG). The non-isothermal simultaneous TG–differential thermal analysis (DTA) of the thermal decomposition of KIO_3 was carried out in nitrogen atmosphere at different heating rates. The isothermal decomposition of KIO_3 was studied using TG at different temperatures in the range 790–805 K in nitrogen atmosphere. The theoretical and experimental mass loss data are in good agreement for the thermal decomposition of KIO_3. The non-isothermal decomposition of KIO_3 was subjected to kinetic analyses by model-free approach, which is based on the isoconversional principle. The isothermal decomposition of KIO_3 was subjected to both conventional (model fitting) and model-free (isoconversional) methods. It has been observed that the activation energy values obtained from all these methods agree well. Isothermal model fitting analysis shows that the thermal decomposition kinetics of KIO_3 can be best described by the contracting cube equation.

Keywords Contracting cube equation · Isothermal decomposition · Model-free methods · Potassium iodate · Thermal decomposition kinetics

Introduction

Thermal decomposition of solids is an important field of solid state chemistry with wide technical applications and has been used to obtain thermal stability parameters of solids [1–4]. The thermal decomposition data generated from TG can be analyzed and manipulated to obtain kinetic parameters such as activation energy (E) and pre-exponential factor (A) [5, 6]. Solid state kinetic data are of practical interest for the large and growing number of technologically important processes. Kinetic studies predict how quickly a system approaches equilibrium and also help to understand the mechanism of the process [7]. A number of reviews are available in the literature on these processes [8–14]. Several authors have emphasized the practical and theoretical importance of information on the kinetics and mechanism of solid state decompositions [15–20].

KIO_3 is a white crystalline powder having a molar mass of 214.001 g which decomposes around 800 K forming potassium iodide (KI) and oxygen. It is sometimes used in radiation treatment, as it can replace radioactive iodine from the thyroid. KIO_3 is used for iodination of table salt and also as an ingredient in baby formula milk. Like potassium bromate, KIO_3 is occasionally used as a maturing agent in baking.

KIO_3 may be used to protect against accumulation of radioactive iodine in the thyroid by saturating the body with a stable source of iodine prior to exposure. KIO_3, when administered at high dosage for extended periods of time, increases the occurrence of tumors in lab rats and has poor shelf life in hot and humid climates. Single-dose, acute toxicity experiments, using KIO_3 showed that iodates cause intoxication and death when administered in sufficient quantities; in some instances, death is attributed to renal damage with retention of non-protein nitrogen [21]. It has been reported that the crystal structure of the I-phase in KIO_3 is *rhombohedral perovskite* and the shorter I–O bond exhibits a covalent bonding character and others (I–K, K–O, and longer I–O bonds) an ionic [22].

K. Muraleedharan (✉) · M. P. Kannan · T. Ganga Devi
Department of Chemistry, University of Calicut, Calicut, Kerala 673 635, India
e-mail: kmuralika@gmail.com

Polyaniline was selectively formed on wool during the polymerization of aniline, using KIO_3 and the infrared (IR) spectrum of polyaniline–wool composite formed shows the presence of cysteic acid units (Cy–SO_3H) resulted from the oxidation of cystine bonds (Cy–S–S–Cy) in wool [23]. The oxidized layer of the wool textiles became thicker and cystine bonds in wool were converted into more cysteic acids by oxidation, using KIO_3 than using $(NH_4)_2S_2O_8$ and $K_2Cr_2O_7$. The formation of polyaniline on wool occurs remarkably in the case of polymerizing aniline, using KIO_3. It has been reported that the addition of KIO_3 to both crude and refined salt resulted in significant darkening and discoloration of most pickled vegetables regardless of the salt source [24].

Henson et al. [25] employed the modified potassium iodate method for the determination of hydrolysable tannins for determining the protein-binding capacity of plant polyphenolics (tannins). Shibli and Saji [26] studied the co-inhibition characteristics of sodium tungstate along with KIO_3 for using it as a corrosion inhibitor in industrial cooling water systems. They carried out detailed studies to investigate the effect of oxygen in the inhibition process and explained the nature and strength of the passive film, and the mechanism of its formation based on the studies conducted under different static and dynamic conditions.

The infant mortality in Xinjiang province, People's Republic of China, which is an area of severe iodine deficiency and has a high infant mortality rate, has been studied by replacing iodine through iodination of the irrigation water [27]. The iodine supplementation of irrigation water in areas of severe iodine deficiency decreases neonatal and infant mortality and observed that iodine replacement has probably been an important factor in the national decrease in infant mortality. Wang et al. [28] studied on the influence of KIO_3 on the metabolism of *Escherichia coli* by intrinsic fluorescence and reported that KIO_3 has great inhibiting effects on the growth of *E. coli* through the pathway of protein synthesis and respiratory chain. As arsenic reacts with KIO_3 (in acidic conditions) to liberate iodine, Revanasiddappa et al. [29] developed a cost-effective and sensitive spectrophotometric method for the determination of arsenic at trace level in environmental samples. Kargosha et al. [30] reported a novel and selective procedure (by injecting KIO_3 solution) for the determination of L-cysteine and L-cystine, in pharmaceutical and urine samples, based on vapor-generation Fourier transform infrared spectrometry (FTIR).

Themelis et al. [31] reported a highly selective and simple flow injection method for the determination of Au(III) in jewel samples, based on the catalytic effect of Au(III) on the oxidation of 4-amino-4′-methoxydiphenylamine hydrochloride (Variamine Blue B base, VB) by KIO_3. They observed that the results obtained using this method agree very well with the results obtained from the reference method, flame atomic absorption spectrometry (FAAS). Suba and Udupa [32] studied the reaction between potassium iodate and molybdenum (VI) oxide in mixtures of different mole ratios employing TG, derivative thermogravimetry (DTG) and DTA techniques in static air atmosphere; followed the kinetics of the reaction and computed the values of *E*. Results of radiosensitization studies by KIO_3 were also reported in the literature [33]. Xiao et al. [34] studied the optical absorption properties of KIO_3 single crystals, calculated the dependence of the absorption coefficient and discussed the characteristics of the absorption edge.

Hegde et al. [35] used slurries containing molybdenum oxide abrasives with KIO_3 as the oxidizing agent to polish copper disks and films, and yielded relatively high removal rates. They reported that the relatively high rates for the removal of copper observed were due to the in situ generation of I_2 by the reaction between KIO_3 and MoO_2. The surface quality of the polished Cu films, however, was very poor with surface roughness values as high as 140 nm. A second polishing using a dilute colloidal silica suspension containing H_2O_2, benzotriazole, and glycine improved the post-polish surface quality, to surface roughness values as low as 0.35 nm [35]. Cherian and Narayana [36] developed a simple and selective spectrophotometric method for the determination of trace amounts of arsenic using azure B as a chromogenic reagent. They observed that the liberated iodine, by the reaction of arsenic (III) with KIO_3, bleaches the violet color of azure B and is measured at 644 nm. This decrease in absorbance is directly proportional to the concentration of As(III), and Beer's law is obeyed in the range 0.2–10 μg mL^{-1} of As(III). They also observed that this method can be successfully applied for the determination of arsenic in various environmental and biological samples.

Objectives of the present investigation

KIO_3 and similar type of compounds have attracted attention due to their technological importance. The thermal decomposition of KIO_3 occurs in the temperature range 795–815 K forming the stable KI [37]. KIO_3 shows an overall decomposition of the type A → B + C, where A and B are solid phases, and C is a gas. Such reactions, typically resulting in highly reactive solid products have attracted a big deal of research due to their theoretical and technical relevance. Even though a vast number of publications are available in the literature on KIO_3 [21–36], studies on the thermal decomposition and kinetics are not available. Industry needs measurements of kinetic parameter for the accurate design of installation and treatment conditions, because augmentation of temperature or elongation of reaction time means more cost. The results of the

kinetic investigations can also be applied to problems as useful lifetime of certain components, oxidative and thermal stability and quality control [38]. The objective of this work is to investigate the thermal decomposition and kinetics of KIO_3 by both isothermal and non-isothermal TG.

Reaction kinetics by TG

The most common experimental technique employed to study kinetics of thermally activated reactions is TG, under the conditions of isothermal and/or non-isothermal conditions. Kinetic studies of thermal decomposition of solids constitute one of the most important applications of thermal analysis. In non-isothermal TG two methods, model fitting and model-free analyses, have been used for the evaluation of kinetic parameters. Model-fitting methods were among the first and most popular methods for kinetic description, because it requires only a single heating rate experiment to calculate the kinetic parameters. However, the popularity of this method has been declined in favor of isoconversional method of model-free approach [39–41].

All kinetic methods assume that the isothermal rate of conversion, $d\alpha/dt$, is a linear function of the temperature dependent rate constant, $k(T)$, and a temperature-independent function of conversion, $f(\alpha)$, which depends on the mechanism of the reaction as:

$$d\alpha/dt = k(T)f(\alpha) \quad (1)$$

The temperature dependent function k(T) is of the Arrhenius type and can be written as (under isothermal conditions):

$$g(\alpha) = kt + C \quad (2)$$

where $g(\alpha)$ is a function, which depends on the mechanism of the reaction. Several kinetic models are available in the literature to describe the mechanism of solid state reactions (see Table 1). The mechanism of the decomposition reaction is usually found out by fitting the TG data into these kinetic models/equations and choosing the model which gives the best fit. The slope of the best fitted line will give k. The kinetic parameters are evaluated by plotting ln k vs. reciprocal temperature (in K).

Under non-isothermal conditions, Eq. 1 becomes:

$$d\alpha/f(\alpha) = (A/\beta)e^{-E/RT}dT \quad (3)$$

where $\beta = dT/dt$, the heating rate. Upon integration and taking logarithms yields

$$\ln g(\alpha) = \ln[AE/\beta R] + \ln p(x) \quad (4)$$

where $p(x) = \int_x^\infty (e^{-x}/x^2)dx$ and $x = E/RT$

This is the basic form of equation used for analysis of non-isothermal data. This equation can be readily applied once the form of the function $p(x)$ is established.

Table 1 Different reaction models used to describe the reaction kinetics

SI. no.	Reaction model	Function, $g(\alpha)$
1	Power law	$\alpha^{1/4}$
2	Power law	$\alpha^{1/3}$
3	Power law	$\alpha^{1/2}$
4	Power law	$\alpha^{3/2}$
5	Exponential law	ln α
6	One-dimensional diffusion	α^2
7	Mampel (first order)	$-\ln(1-\alpha)$
8	Avrami–Erofeev	$[-\ln(1-\alpha)]^{1/4}$
9	Avrami–Erofeev	$[-\ln(1-\alpha)]^{1/3}$
10	Avrami–Erofeev	$[-\ln(1-\alpha)]^{1/2}$
11	Avrami–Erofeev	$[-\ln(1-\alpha)]^{2/3}$
12	Three-dimensional diffusion	$[1-(1-\alpha)^{1/3}]^2$
13	Contracting sphere	$1-(1-\alpha)^{1/3}$
14	Contracting area (cylinder)	$1-(1-\alpha)^{1/2}$
15	Second order	$(1-\alpha)^{-1}-1$
16	Prout–Tompkins	$\ln[\alpha/(1-\alpha)]$

For kinetic analyses, the main task is to get the solution of the above temperature integral. Several methods are available under different approaches, viz., integral, differential and approximation, for the evaluation of the temperature integral. However, most of the approximation methods neglect the low temperature end of the temperature integral. It has been reported that two-dimensional quantities significantly influence the approximation methods [42], and the solution of the temperature integral is achieved by numerical integration with respect to a dimensionless activation energy variable [43].

The model-free method

Measuring the evolution of overall physical properties of a system, by thermal methods of analysis, provides information on macroscopic kinetics. The macroscopic kinetics is inherently complex, because they include information about multiple steps that occur simultaneously. Unscrambling complex kinetics presents a serious challenge that can only be met by kinetic methods that provide means of detecting and treating multistep processes. Isoconversional methods, based on multiple heating programmes, are the most popular methods that can meet this challenge [44].

Isoconversional kinetics rests upon evaluating a dependence of the effective activation energy on conversion or temperature and using this dependence for making kinetic predictions and for exploring the mechanism of thermal processes. These methods are based on the single-step kinetic equation, Eq. 3, of non-isothermal decomposition and are the quickest way to derive kinetic parameters for

complex reactions involving multiple processes [45]. According to isoconversional principle, at a constant extent of conversion, the reaction rate is a function only of temperature so that:

$$\mathrm{d}[\ln(\mathrm{d}\alpha/\ \mathrm{d}t)]_{\alpha}/\ \mathrm{d}T^{-1} = E_{\alpha}/RT \quad (5)$$

the subscript α designates the value related to a given value of conversion

The isoconversional method suggested by Flynn–Wall–Ozawa [46] uses approximation of the integral equation, which leads to simple linear equation for evaluation of E. This method assumes that the conversion function does not change with the alteration of heating rate for all values of α, i.e., measurement of temperature corresponding to fixed values of α at different heating rate is required. Under these conditions Eq. 3 becomes:

$$\ln \beta = \ln[Af(\alpha)]/[\mathrm{d}\alpha/\mathrm{d}t] - E/RT \quad (6)$$

and a plot of ln β vs. $1/T$ should give a straight line with a slope of $(-E/R)$.

If the values of E determined for the various values of α, are almost constant, then certainly the reaction involves only a single step. On the contrary, a change in E with increasing degree of conversion is an indication of a complex reaction mechanism that invalidates the separation of variables involved in the Ozawa, Flynn, and Wall analysis [47]. These complications are serious, especially in the case where the total reaction involves competitive reaction mechanisms [48].

Model-free kinetics rests on evaluating the E_{α} dependence, which is adequate for both theoretical and practical purposes of kinetic predictions [49]. Normally, model-free kinetics does not concern with evaluating A and $g(\alpha)$ or $f(\alpha)$ because they are not needed for performing kinetic predictions. Also, these values are hardly suitable for theoretical interpretation because of the strong ambiguity associated with them. However, these values can be determined in the frameworks of model-free kinetics.

Experimental

AnalaR grade KIO_3 of *E* merck is dissolved in water, recrystalized, dried, powdered in an agate mortar, fixed the particle size in the ranges, 90–106 μm and kept in a vacuum desiccator. Non-isothermal TG–DTA analyses of KIO_3 samples were carried out on a SETARAM made Labsys TG-DTA-1600 at four different heating rates, viz, 3, 5, 7, and 10 K min^{-1}. The isothermal TG measurements were carried out using the same instrument at different temperatures, viz., 790, 795, 800, and 805 K. The operational characteristics of the TG–DTA system are; atmosphere: flowing nitrogen, at a flow rate of 60 mL min^{-1}, sample mass: 10 mg, sample pan: silica. Duplicate run's were made under similar conditions and found that the data overlap with each other, indicating satisfactory reproducibility.

Results and discussion

Preview of earlier work

Solymosi reported that the thermal decomposition reaction of KIO_3, at one atmosphere pressure and in the temperature range 485–520 °C, is autocatalytic and observed rapid reaction up to 25–30% conversion; beyond which the reaction suddenly slows down and shows a maximum rate around 26% conversion [50]. The Prout–Tompkins [51] equation proved to be the most suitable for kinetic analysis of the decomposition curve; E values of 258 and 224 kJ mol^{-1} were reported for the acceleratory and the

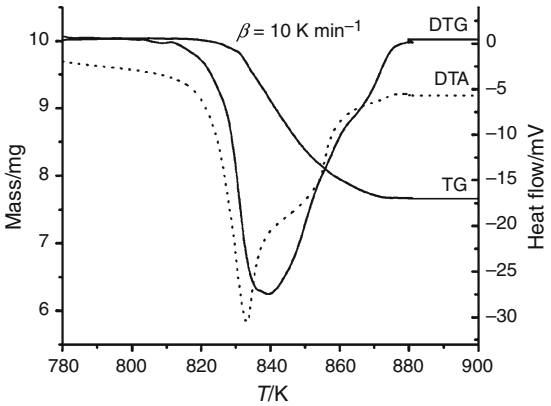

Fig. 1 Simultaneous TG–DTG–DTA curve for the thermal decomposition of KIO_3 at 10 K min^{-1}

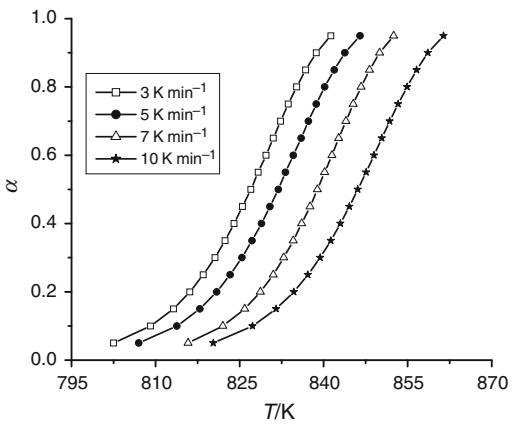

Fig. 2 α–T curve for the thermal decomposition of KIO_3 at different temperatures

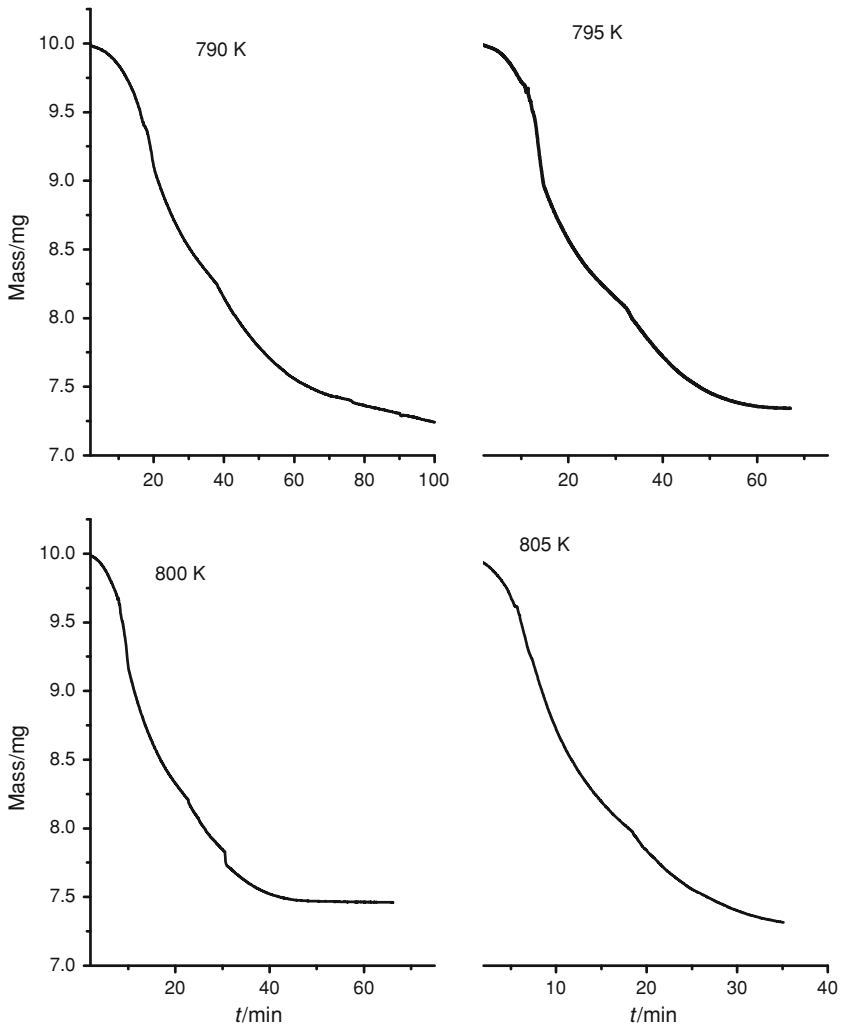

Fig. 3 Isothermal decomposition of KIO_3 at different temperatures

decay period, respectively. Chloride, bromide, and iodide ions exerted considerable acceleratory effects on the reaction [50]. At higher temperatures the decomposition was found to be of deceleratory in nature; at lower temperatures the rate maximum occurred at smaller conversions. The presence of halides decreased the activation energy of the thermal decomposition reaction. Nickel oxide effectively catalyzed the decomposition. In this case too the decomposition started with the highest rate. The first order equation was found to be the most suitable for the calculation of rate constant of the catalytic reaction. The value of the E observed was 216 kJ mol^{-1}.

Nuclear quadrupole resonance of KIO_3 indicated that KIO_3 behaves quite differently from the other alkali metal iodates. It is ferroelectric below 212 °C and undergoes four phase transitions, at −190, −10, 75, and 220 °C [50, 52]. Above 220 °C, the symmetry is rhombohedral (a = 9.012 Å, $\alpha = 89° 14'$). Below this temperature, some trigonal lines show further splitting; caused by deviation from the trigonal symmetry of the high temperature triclinic form. Salje [53] found that phase transitions of first order

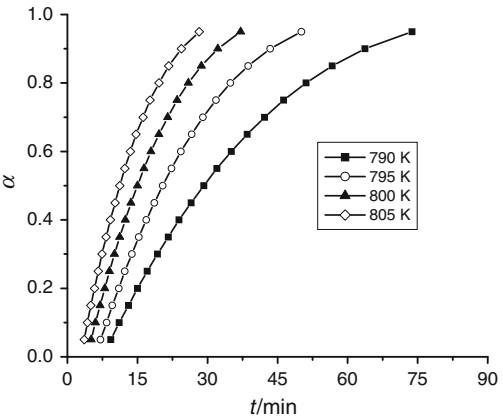

Fig. 4 α–t curves for the thermal decomposition of KIO_3 at different temperatures

occurred at −163, −15, 72.5, and 214 °C. Pure quadrupole resonance of ^{127}I has been detected in all the alkali metal iodates, showing that none of them has a perovskite-like structure [50]. Based on this and additional DTA

investigations, it is concluded that KIO_3 has at least two monoclinic, two rhombohedral and one triclinic modification, and it is very likely that several modifications of KIO_3 exist together at room temperature, readily transforming from one to another [54]. This could be the reason why the lattice of KIO_3 contains many faults and the diffractograms of different preparations are slightly different.

It has been reported [55] that iodates of alkali metals (except Li), Ag, Co and probably Hg(I) and Hg(II) decompose according to:

(a) $2\ IO_3^- \rightarrow 2\ I^- + 3O_2$; iodates of Cu, Cd, Zn, Ni and probably Mg, Ti(I), and Pb go to the oxide through,

(b) $4IO_3 \rightarrow 2O^{2-} + I_2 + 5O_2$, iodates of Na and K also go partly with this route, and iodates of Li, Ca, Ba, Sr and rare earth form orthoperiodate as,

(c) $5\ IO_3^- \rightarrow IO_5^- + 5O_2 + 2\ I_2$

Reactions of the type (a) for Na, K, Rb, and Cs attain equilibrium and these constants were calculated, no calculations were carried out for type (b) reactions but for

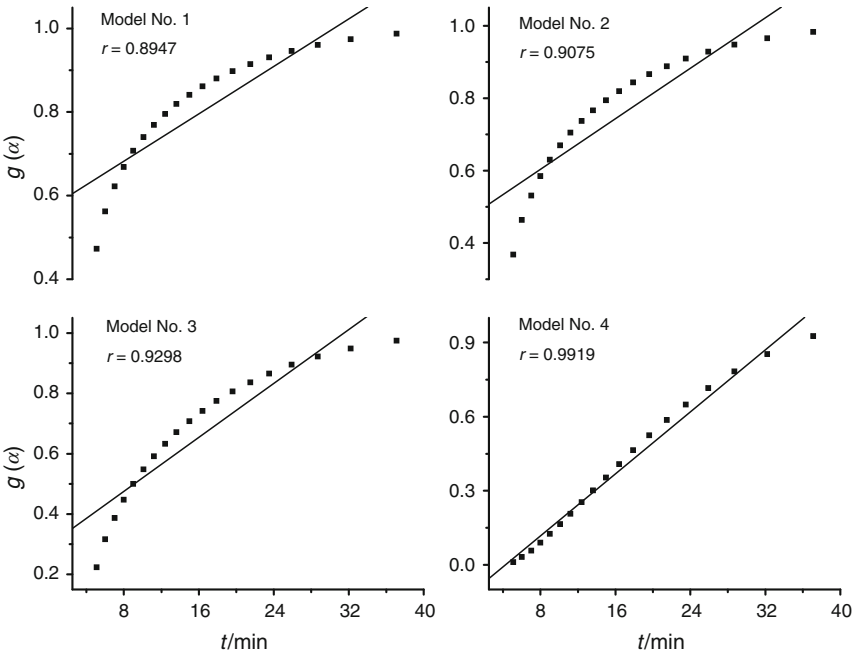

Fig. 5 Typical model fits for the isothermal decomposition of KIO_3 at 795 K

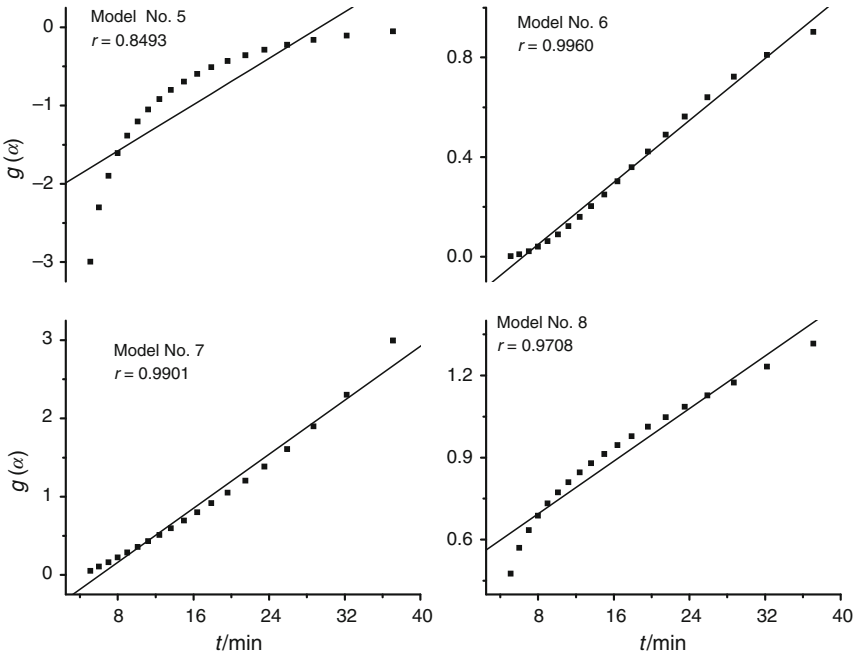

Fig. 6 Typical model fits for the isothermal decomposition of KIO_3 at 795 K

reactions of type (c) calculations were made only for Ca since no S^0 (298 K) values for the periodates of Li, Ba, and Sr are available [55].

Thermal decomposition of KIO_3

Figure 1 shows the TG–DTG–DTA curves for KIO_3 at a heating rate of 10 K min^{-1} in nitrogen atmosphere. Similar curves were obtained for the thermal decomposition of KIO_3 at heating rates of 3, 5, and 7 K min^{-1} (not shown). It has been observed that KIO_3 decomposes around 800 K forming KI by releasing oxygen. The energetics and kinetics, of the thermal decomposition of KIO_3, have been studied by applying model-free method of kinetic analysis. The α–T curves for the non-isothermal decomposition of KIO_3 at different heating rates are shown in Fig. 2. The observed mass changes for the decomposition agree very well with the theoretical values for all samples of KIO_3 at all heating rates. The isothermal TG (at different temperatures) and α–t curves for the isothermal decomposition of KIO_3 are shown, respectively, in Figs. 3 and 4.

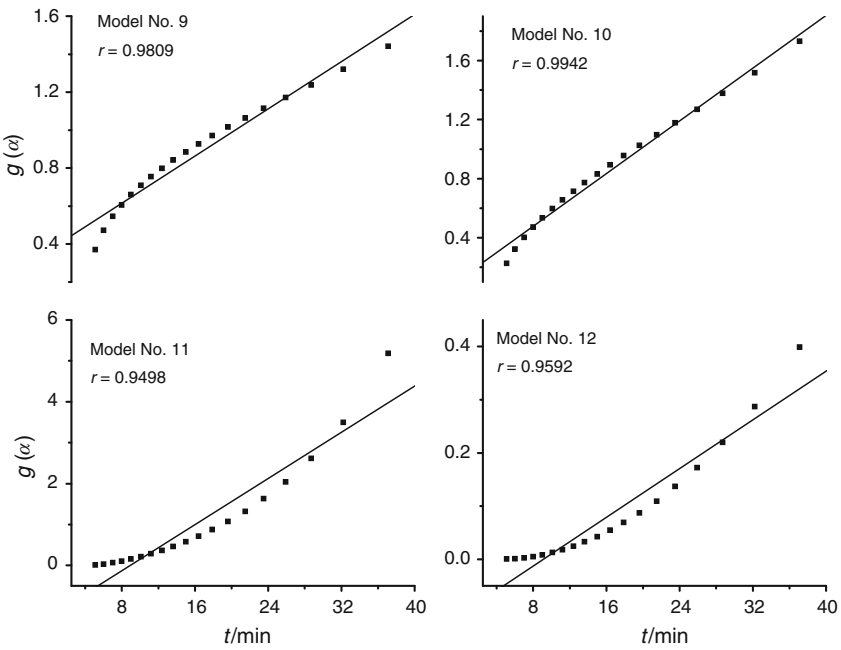

Fig. 7 Typical model fits for the isothermal decomposition of KIO_3 at 795 K

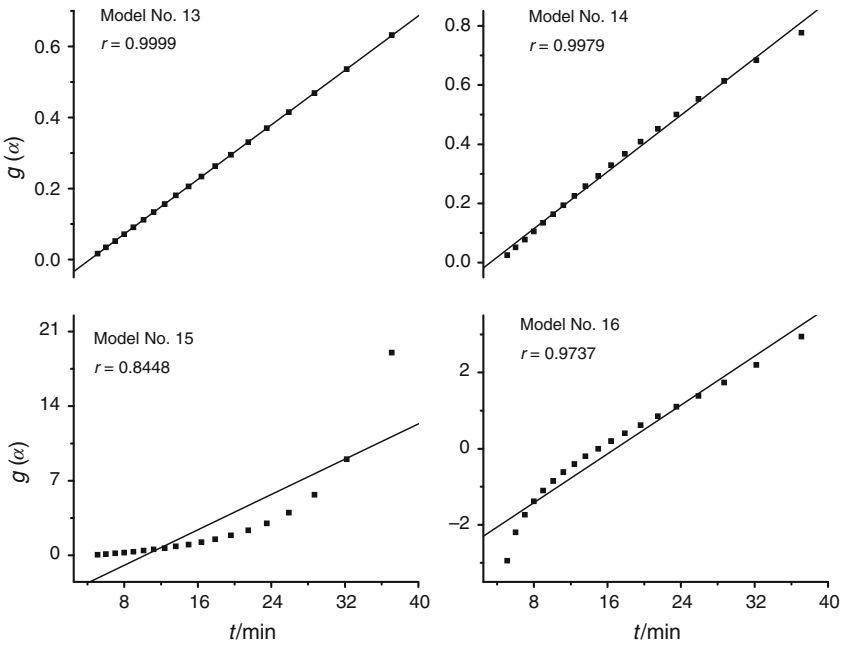

Fig. 8 Typical model fits for the isothermal decomposition of KIO_3 at 795 K

Table 2 Values of slope, correlation coefficient (r) obtained from isothermal model fitting to different equations at different temperatures

Model no.	Temperature/K							
	790		795		800		805	
	Slope/min^{-1}	r	Slope/min^{-1}	r	Slope/min^{-1}	r	Slope/min^{-1}	r
1	0.0070	0.8946	0.0106	0.8946	0.0142	0.8947	0.0185	0.8950
2	0.0087	0.9074	0.0130	0.9075	0.0174	0.9075	0.0227	0.9079
3	0.0111	0.9298	0.0167	0.9298	0.0223	0.9298	0.0291	0.9302
4	0.0156	0.9919	0.0234	0.9918	0.0314	0.9920	0.0408	0.9920
5	0.0368	0.8492	0.055	0.8493	0.0740	0.8493	0.0963	0.8497
6	0.0155	0.9959	0.0232	0.9959	0.0311	0.9960	0.0405	0.9959
7	0.0429	0.9902	0.0644	0.9902	0.0862	0.9901	0.1122	0.9900
8	0.0119	0.9707	0.0179	0.9708	0.0240	0.9708	0.0312	0.9710
9	0.0154	0.9811	0.0232	0.9809	0.0311	0.9809	0.0404	0.9811
10	0.0225	0.9942	0.0333	0.9942	0.0446	0.9942	0.0580	0.9943
11	0.0701	0.9501	0.1052	0.9502	0.1410	0.9498	0.1834	0.9497
12	0.0057	0.9593	0.0086	0.9594	0.0115	0.9590	0.0149	0.9590
13	0.0095	**0.9999**	0.0143	**0.9999**	0.0192	**0.9999**	0.0250	**0.9999**
14	0.0119	0.9979	0.0179	0.9979	0.0240	0.9979	0.0312	0.9980
15	0.2062	0.8455	0.3097	0.8457	0.4146	0.8448	0.5395	0.8448
16	0.0796	0.9737	0.1196	0.9738	0.1602	0.9737	0.2085	0.9739

Bold values indicate the maximum correlation coefficient

Table 3 Values of slope and correlation coefficient (r) obtained from isothermal model fitting to different equations for the thermal decomposition region, $\alpha = 0.05$–0.5

Reaction model	790 K		795 K		800 K		805 K	
	Slope/min^{-1}	r	Slope/min^{-1}	r	Slope/min^{-1}	r	Slope/min^{-1}	r
1	0.0171	0.9598	0.0256	0.9600	0.0345	0.9610	0.0446	0.9597
2	0.0200	0.9671	0.0300	0.9672	0.0404	0.9681	0.0522	0.9669
3	0.0233	0.9791	0.0349	0.9792	0.0469	0.9800	0.0607	0.9790
4	0.0175	0.9978	0.0263	0.9978	0.0354	0.9975	0.0458	0.9979
5	0.1026	0.9334	0.1539	0.9337	0.2071	0.9349	0.2677	0.9331
6	0.0126	0.9862	0.0189	0.9862	0.0255	0.9855	0.0330	0.9863
7	0.0322	0.9996	0.0483	0.9996	0.0649	0.9994	0.0840	0.9995
8	0.0206	0.9745	0.0308	0.9746	0.0415	0.9754	0.0537	0.9743
9	0.0245	0.9810	0.0367	0.9811	0.0494	0.9818	0.0638	0.9808
10	0.0294	0.9909	0.0441	0.9910	0.0594	0.9914	0.0768	0.9908
11	0.0318	0.9970	0.0477	0.9970	0.0642	0.9973	0.0830	0.9970
12	0.0021	0.9721	0.0032	0.9721	0.0042	0.9713	0.0055	0.9721
13	0.0095	**0.9999**	0.0143	**0.9999**	0.0192	**0.9999**	0.0248	**0.9999**
14	0.0135	**0.9999**	0.0202	**0.9999**	0.0271	**0.9999**	0.0351	**0.9999**
15	0.0469	0.9928	0.0703	0.9928	0.0945	0.9924	0.1224	0.9927
16	0.1347	0.9614	0.2021	0.9616	0.2720	0.9625	0.3517	0.9612

Bold values indicate the maximum correlation coefficient

Kinetics of thermal decomposition

The method of model fitting

The α–t data in the range $\alpha = 0.05$–0.95 of the isothermal decomposition of KIO_3 were subjected to weighted least squares analysis using various kinetic reaction models given in Table 1. Typical model fitting plots, for various models given in Table 1, for the thermal decomposition of KIO_3 in the range $\alpha = 0.05$–0.95 at 795 K are shown in Figs. 5, 6, 7, and 8. Similar types of curves were obtained at all other temperatures studied (not shown). The values of

Table 4 Values of slope and correlation coefficient (r) obtained from isothermal model fitting to different equations for the thermal decomposition region, $\alpha = 0.5$–0.95

Reaction model	790 K		795 K		800 K		805 K	
	Slope/min^{-1}	r	Slope/min^{-1}	r	Slope/min^{-1}	r	Slope/min^{-1}	r
1	0.0033	0.9653	0.0049	0.9648	0.0066	0.9659	0.0086	0.9654
2	0.0042	0.9671	0.0064	0.9666	0.0085	0.9677	0.0111	0.9672
3	0.0060	0.9706	0.0090	0.9702	0.0121	0.9712	0.0158	0.9707
4	0.0132	0.9871	0.0198	0.9869	0.0265	0.9876	0.0345	0.9873
5	0.0142	0.9595	0.0214	0.9590	0.0287	0.9601	0.0373	0.9596
6	0.0151	0.9926	0.0227	0.9924	0.0304	0.9930	0.0396	0.9927
7	0.0503	0.9937	0.0756	0.9939	0.1012	0.9933	0.1319	0.9936
8	0.0090	0.9987	0.0134	0.9986	0.0180	0.9988	0.0235	0.9987
9	0.0124	0.9994	0.0186	0.9994	0.0249	0.9995	0.0324	0.9994
10	0.0199	0.9999	0.0299	0.9999	0.0400	0.9998	0.0522	0.9998
11	0.0286	0.9991	0.0429	0.9991	0.0575	0.9989	0.0749	0.9990
12	0.0078	0.9887	0.0118	0.9890	0.0158	0.9883	0.0205	0.9886
13	0.0095	**0.9999**	0.0143	**0.9999**	0.0192	**0.9999**	0.0250	**0.9999**
14	0.0109	0.9985	0.0164	0.9984	0.0220	0.9987	0.0287	0.9986
15	0.3469	0.9058	0.5212	0.9063	0.6969	0.9042	0.9090	0.9052
16	0.0645	0.9994	0.0969	0.9995	0.1299	0.9993	0.1692	0.9994

Bold values indicate the maximum correlation coefficient

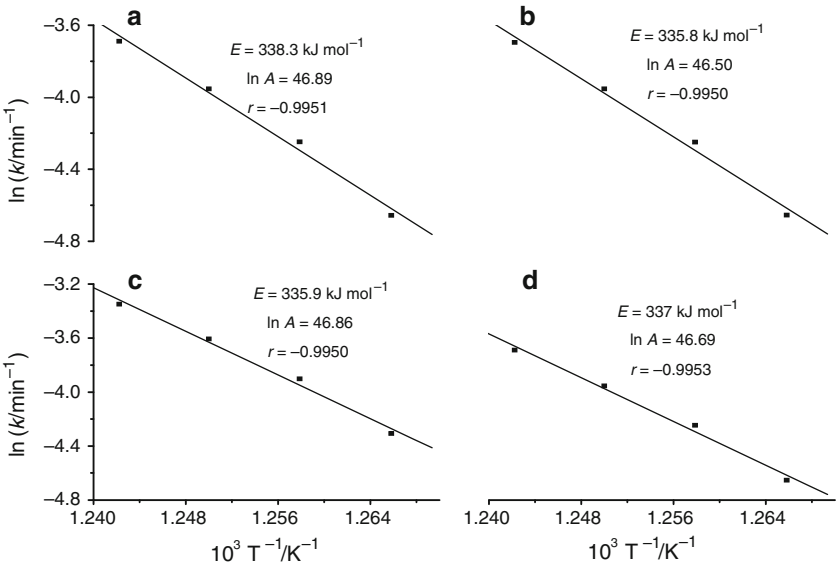

Fig. 9 Arrhenius plot for the thermal decomposition of KIO_3. Model no. 13: **a** ($\alpha = 0.05$–0.95), **b** ($\alpha = 0.05$–0.5), **d** ($\alpha = 0.5$–0.95) and Model no. 14: **c** ($\alpha = 0.05$–0.5)

slope and correlation coefficient (r) obtained by weighted least squares plot at 790, 795, 800, and 805 K for all kinetic models are given in Table 2. Perusal of Table 2 and Figs. 5, 6, 7, and 8 shows that the contracting cube equation, $1 - (1 - \alpha)^{1/3} = kt$, gave the best fits ($r = 0.9999$) at all temperatures studied. Separate kinetic analysis of the α–t values corresponding to the ranges $\alpha = 0.05$–0.5 and $\alpha = 0.5$–0.95 showed that the former range gave the best fits to both contracting cube and contracting area models whereas the latter range gave best fits to the contracting cube model. Description of reaction kinetics using different rate laws for different ranges of α is not unusual in solid-state reactions. For instance Philips and Taylor used Prout–Tompkins equation to describe the acceleratory region of the decomposition of KIO_4 and the contracting cube equation for the decay stage [56]. It has also been reported that under isothermal conditions KIO_4 decomposes via two stages; the Prout–Tompkins equation best describes the acceleratory stage and the deceleratory stage proceeds according to contracting area law [57–59]. The

Table 5 Values of slope, E, r, and % deviation (in E) obtained from model-free analysis at different conversions

Conversion/%	Slope/K^{-1}	E/kJ mol^{-1}	$-r$	% Deviation in E^a
10	41.37	344.0	0.9834	1.62
15	41.78	347.3	0.9839	0.65
20	41.70	346.7	0.9847	0.84
25	41.82	347.7	0.9846	0.55
30	41.97	348.9	0.9844	0.19
35	42.01	349.3	0.9841	0.10
40	42.15	350.4	0.9847	−0.23
45	42.09	349.9	0.9844	−0.09
50	42.35	352.1	0.9840	−0.71
55	42.05	349.6	0.9833	0.00
60	42.24	351.1	0.9830	−0.44
65	42.31	351.8	0.9832	−0.62
70	42.22	351.0	0.9828	−0.41
75	42.18	350.7	0.9820	−0.31
80	42.14	350.3	0.9811	−0.21
85	42.22	351.0	0.9810	−0.40
90	42.21	350.9	0.9799	−0.37
95	42.14	350.4	0.9791	−0.22

Average value of $E = 349.6$. [a] From average value of E

acceleratory stage in the decomposition of Lithium perchlorate followed Prout–Tompkins rates law whereas the decay stage followed the monomolecular model [60]. Similarly both the acceleratory and decay regions of the thermal decomposition of sodium perchlorate and of potassium bromate were well described by the Prout-Tompkins relation with separate rate constants [50]. It has also been reported that $KBrO_3$ decomposes in two stages, both stages following the contracting area equation but with different rate constants [61]. Kim et al. [62] has reported that the reaction model varies with reaction temperature in isothermal pyrolysis of polypropylene and they observed that the Arrhenius parameters derived from the assumptions of nth order model would be improper.

The values of slope and r obtained from least squares fits for various reaction models given in Table 1 for both ranges of the isothermal decomposition of KIO_3 are given in Tables 3 and 4. Values of E, A, and r are shown in the Arrhenius plots, for the ranges $\alpha = 0.05$–0.95, $\alpha = 0.05$–0.5 and $\alpha = 0.5$–0.95, of the isothermal decomposition of KIO_3 (Fig. 9). It has been found that the values of E obtained for the different ranges of α and for the two models, contracting cube and contracting square, remain within 337.2 ± 1.8 kJ mol^{-1}.

The model-free approach

The apparent activation energy values were also estimated by the isoconversional method suggested by Ozawa, Flynn, and Wall [47] for the thermal decomposition of KIO_3 at different percentage of conversion by fitting the plots of ln β versus $1/T$ and are given in Table 5 along with the values of slope, r and percentage deviation in E. Table 5 shows that the isoconversional plots for the thermal decomposition of KIO_3 at all percentages of conversions give high values of r (~ -0.9999) with E values of 348 ± 4 kJ mol^{-1}. Typical isoconversional plots for the thermal decomposition of

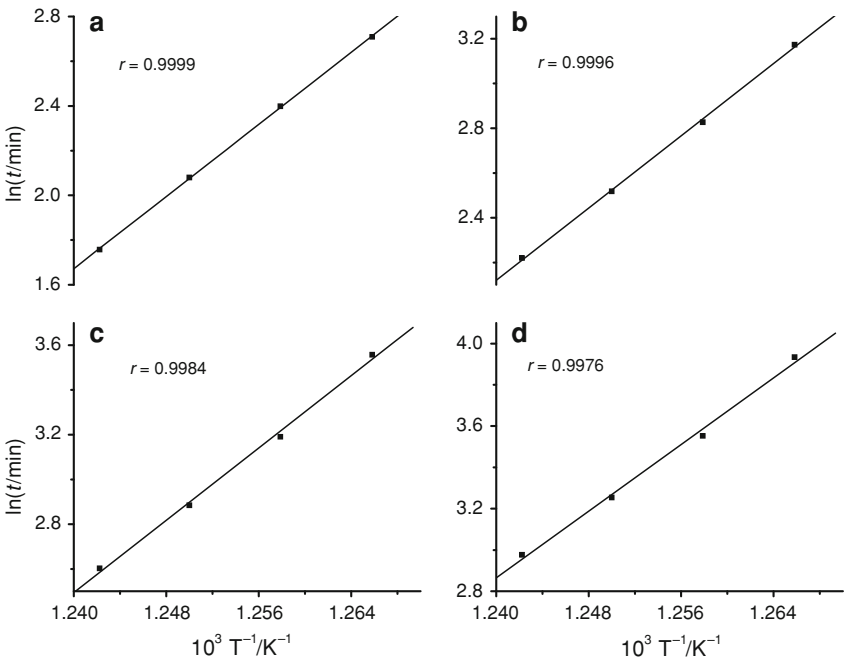

Fig. 10 Typical isoconversional plots for the thermal decomposition of KIO_3 at different conversions (**a** = 20%, **b** = 40%, **c** = 60%, **d** = 80%)

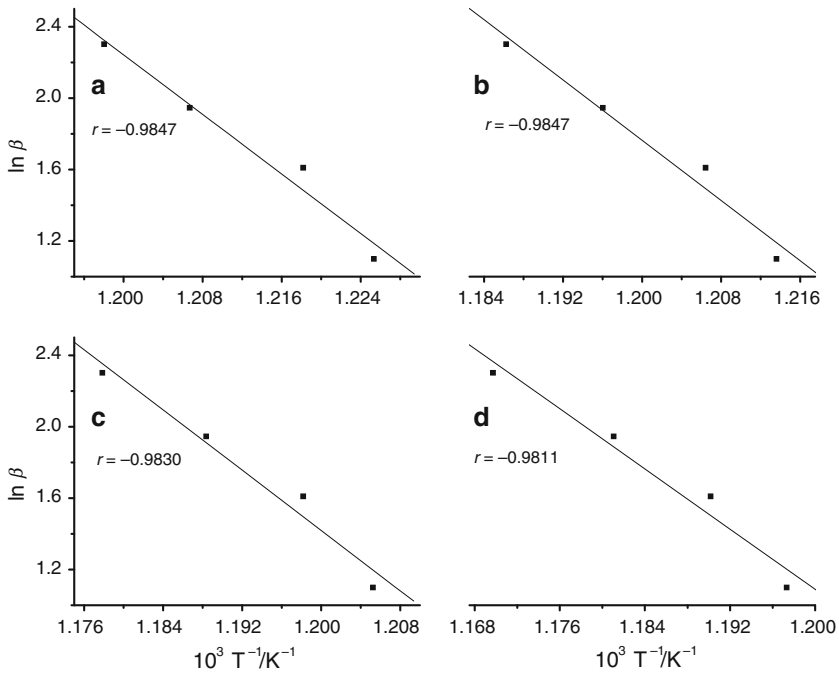

Fig. 11 Typical isoconversional plots for the thermal decomposition of KIO_3 at different conversions (**a** $\alpha = 0.2$, **b** $\alpha = 0.4$, **c** $\alpha = 0.6$, **d** $\alpha = 0.8$)

KIO_3 are shown in Fig. 10. The apparent activation energy values determined for the various values of conversion show little deviation indicating that the thermal decomposition of KIO_3 proceeds through a single step.

The α–t data, in the range of $\alpha = 0.05$–0.95, of the isothermal decomposition of KIO_3 were also subjected to isoconversional studies for the determination of apparent activation energy as a function of α from the sets of isothermals obtained. A plot of ln t (t being the time required for reaching a given value of α at a constant temperature T) versus the corresponding reciprocal of the temperature ($1/T$) would lead to E for the given value of α. Typical isothermal isoconversional plots are shown in Fig. 11. The results are given in Table 6. A perusal of Table 6 reveals that the values E obtained for different values α lies in the range of 335–339 kJ mol^{-1}, which is in good agreement with those obtained from conventional method.

Table 6 Values of slope, E and correlation coefficient (r) obtained from isothermal isoconversional analysis at different conversions

α	Slope/K^{-1}	E/kJ mol^{-1}	r
0.05	40.41	336.0	0.9981
0.10	40.46	336.3	0.9989
0.15	40.76	338.9	0.9997
0.20	40.30	335.1	0.9999
0.25	40.30	335.1	0.9999
0.30	40.55	337.1	0.9999
0.35	40.47	336.5	0.9996
0.40	40.37	335.7	0.9996
0.45	40.42	336.1	0.9992
0.50	40.48	336.6	0.9991
0.55	40.40	335.9	0.9989
0.60	40.36	335.6	0.9984
0.65	40.63	337.8	0.9986
0.70	40.35	335.5	0.9981
0.75	40.55	337.1	0.9981
0.80	40.37	335.7	0.9976
0.85	40.47	336.4	0.9976
0.90	40.43	336.1	0.9974
0.95	40.55	337.1	0.9971

Mechanism of thermal decomposition

This study revealed that the thermal decomposition of KIO_3 undergoes through contracting cube equation with an E value of $\sim$340 kJ mol^{-1}. Separate kinetic analysis of the α–t values corresponding to the range $\alpha = 0.05$–0.5 showed that this range gave the best fits to both contracting cube and contracting area models. Both the models, contracting cube and contracting area, are deceleratory in nature. According to contracting cube model, the initial nucleation occurs rapidly over all surfaces for a single cube of the reactant and the interface established progresses thereafter in the direction of the centre of the crystal, reaction is deceleratory throughout since the reaction interface progressively decreases. But in the case of contracting area model, the interface established progresses in the direction of the centre of the crystal with a progressive decrease in contact area. Initially nucleation and growth of the reactant, KIO_3, take place in two/three-dimensional

way, as time passes the three-dimensional way of reaction predominates over the two-dimensional way and becomes purely three dimensional above $\alpha = 0.5$. This may be the reason for obtaining best fits for both contracting cube and contracting area models below $\alpha = 0.5$.

Conclusions

Earlier workers observed that both Prout–Tompkins and first-order equation describes the thermal decomposition of KIO_3 [50]. Prout-Tompkins equation is autocatalytic, while first-order equation is deceleratory in nature. The present investigation revealed that the thermal decomposition of KIO_3 proceeds according to contracting cube equation, which is deceleratory in nature. Model-fitting analysis shows that both Prout–Tompkins and first-order models gave poor correlation for the thermal decomposition of KIO_3 (see Tables 2, 3, 4; Figs. 5, 6, 7, 8). The rate of solid state reactions is usually controlled either by *electron transfer*, or *diffusion* (of ions in the lattice) mechanism. Electron transfer mechanism involves the transfer of an electron from the iodate anion to potassium cation to form the free radicals $K^{\bullet}$ and $IO_3^{\bullet}$. As $IO_3^{\bullet}$ involves a one-electron bond, it is very unstable and readily decomposes to give $O^{\bullet}$ and relatively stable $I^{\bullet}$. Two $O^{\bullet}$ species combine to give one oxygen molecule. $I^{\bullet}$ is stabilized by receiving an electron from $K^{\bullet}$ forming KI. In the case of diffusion mechanism, the diffusion of the similarly sized cation and/or anion [63] toward potential sites is the rate-determining step of the decomposition; at the potential sites, these ions undergo spontaneous reaction producing highly reactive radicals, which break down to form solid KI and gaseous oxygen. Further investigations, such as pretreatment studies, are required to clearly establish the mechanism, the rate determining step, of the thermal decomposition of KIO_3.

Acknowledgements The authors are thankful to KSCSTE for providing instrumental facility.

References

1. Vecchio S, Rodante F, Tomasssetti M. Thermal stability of disodium and calcium phosphomycin and the effects of the excipients evaluated by thermal analysis. J Pharma Biomed Anal. 2000;24:1111–23.
2. Huang Y, Cheng Y, Alexander K, Dollimore D. The thermal analysis study of the drug captopril. Thermochim Acta. 2001;367:43–58.
3. Dollimore D, O'Connell C. A comparison of the thermal decomposition of preservatives using thermogravimetry and rising temperature kinetics. Thermochim Acta. 1998;324:33–48.
4. Halikia I, Neou-Syngouna P, Kolitsa D. Isothermal kinetic analysis of the thermal decomposition of magnesium hydroxide using thermogravimetric data. Thermochim Acta. 1998;320:75–88.
5. Vyazovkin S, Wight CA. Model-free and model-fitting approaches to kinetic analysis of isothermal and nonisothermal data. Thermochim Acta. 1999;340–341:53–68.
6. Rodante F, Vecchio S, Tomassetti M. Kinetic analysis of thermal decomposition for penicillin sodium salts: model-fitting and model-free methods. J Pharm Biomed Anal. 2002;29:1031–43.
7. Malek J, Mitsuhashi T, Criado JM. Kinetic analysis of solid-state processes. J Mater Res. 2001;16:1862–71.
8. Benderskii VA, Makarov DE, Wight CA. Chemical dynamics at low temperatures. New York: Wiley; 1994. p. 385.
9. Brown ME, Dollimore D, Galwey AK. Reactions in the solid state, comprehensive chemical kinetics, vol. 22. Amsterdam: Elsevier; 1980. p. 340.
10. Brill TB, James KJ. Kinetics and mechanisms of thermal decomposition of nitroaromatic explosives. Chem Rev. 1993;93:2667–92.
11. Flynn JH. Thermal analysis. In: Mark HF, Bikales NM, Overberger CG, Menges G, editors. Encyclopedia of polymer science and engineering. NewYork: Wiley; 1989. p. 690.
12. Fatou JG. Crystallization kinetics. In: Mark HF, Bikales NM, Overberger CG, Menges G, editors. Encyclopedia of polymer science and engineering. New York: Wiley; 1989. p. 231.
13. Galwey AK. Is the science of thermal analysis kinetics based on solid foundations? A literature appraisal. Thermochim Acta. 2004;413:139–83.
14. Dollimore D. Thermal analysis. Anal Chem. 1996;68:63–72.
15. Galwey AK, Brown ME. Thermal decomposition of ionic solids. Amsterdam: Elsevier; 1999.
16. Vyazovkin S. Kinetic concepts of thermally stimulated reactions in solids: a view from a historical perspective. Int Rev Phys Chem. 2000;19:45–60.
17. Kotler JM, Hinman NW, Richardson CD, Scott JR. Thermal decomposition behaviour of potassium and sodium jasorite synthesized in the presence of methyl amine and alanine. J Therm Anal Calorim. 2010;102:23–9.
18. Bertol CD, Cruz AP, Stulzer HK, Murakami FS, Silva MAS. Thermal decomposition kinetics and compatibility studies of primaquine under isothermal and non-isothermal conditions. J Therm Anal Calorim. 2010;102:187–92.
19. Bayram H, Önal M, Hamza Y, Sarıkaya Y. Thermal analysis of a white calcium bentonite. J Therm Anal Calorim. 2010;101:873–9.
20. Cabrales L, Abidi N. On the thermal degradation of cellulose in cotton fibers. J Therm Anal Calorim. 2010;102:485–91.
21. Webster SH, Rice ME, Highman B, Von Oettingen WF. The toxicology of potassium and sodium iodates: acute toxicity in mice. J Pharmacol Exp Ther. 1957;120:171–8.
22. Kasatani H, Aoyagi S, Kuroiwa Y, Yagi K, Katayama R, Terauchi H. Study of crystal structure at high temperature phase in KIO_3 crystal by synchrotron powder X-ray diffraction. Nucl Instr Methods Phys Res Sect B. 2003;199:49–53.
23. Hirase R, Shikata T, Shirai M. Selective formation of polyaniline on wool by chemical polymerization, using potassium iodate. Synth Met. 2004;146:73–7.
24. Amr AS, Jabay OA. Effect of salt iodization on the quality of pickled vegetables. J Food Agric Environ. 2004;2:151–6.
25. Henson GL, Niemeyer L, Ansong G, Forkner R, Makkar HPS, Hagerman AE. A modified method for determining protein binding capacity of plant polyphenolics using radiolabelled protein. Phytochem Anal. 2004;15:159–63.
26. Shibli SMA, Saji VS. Co-inhibition characteristics of sodium tungstate with potassium iodate on mild steel. Corros Sci. 2005;47:2213–24.

27. DeLong GR, Leslie PW, Wang S, Jiang X, Zhang M, Rakeman M, Jiang J, Ma T, Cao X. Effect on infant mortality of iodination of irrigation water in a severely iodine-deficient area of China. Lancet. 1997;350:771–3.
28. Wang H, Wang J, Xu J, Cai R. Study on the influence of potassium iodate on the metabolism of *Escherichia coli* by intrinsic fluorescence. Spectrochim Acta A. 2006;64:316–20.
29. Revanasiddappa HD, Dayananda BP, Kumar TNK. A sensitive spectrophotometric method for the determination of arsenic in environmental samples. Environ Chem Lett. 2007;5:151–5.
30. Kargosha K, Ahmadi SH, Zeeb M, Moeinossadat SR. Vapour phase fourier transform infrared spectrometric determination of L-cysteine and L-cystine. Talanta. 2008;74:753–9.
31. Themelis DG, Trellopoulos AV, Tzanavaras PD, Sofoniou M. Highly selective flow injection spectrophotometric determination of gold based on its catalytic effect on the oxidation of variamine blue by potassium iodate in aqueous *N*,*N*-dimethylformamide medium. Talanta. 2007;72:277–81.
32. Suba K, Udupa MR. Solid state reactions in the potassium iodate and molybdenum(VI) oxide system. J Therm Anal Calorim. 1989;35:1191–5.
33. Kada T. Radiosensitization by potassium iodate and related compounds. Int J Rad Biol. 1969;15:271–4.
34. Xiao DQ, Wang X, Zheng WC, Lu MK. Optical absorption properties of potassium iodate single crystals. Ferroelectrics. 1989;100:213–21.
35. Hegde S, Udaya BP, Babu SV. Chemical-mechanical polishing of copper using molybdenum dioxide slurry. J Mater Res. 2005; 20:2553–61.
36. Cherian T, Narayana B. A new spectrophotometric method for the determination of arsenic in environmental and biological samples. Anal Lett. 2005;38:2207–16.
37. Breusov ON, Kashina NJ, Rezvina TV. Thermal decomposition of chlorates, bromates, iodates, perchlorates and periodates of potassium, rubidium and cesium. Zh Neorg Khim. 1970;15: 612–4.
38. Celis K, Driessche IV, Mouton R, Vanhoyland G, Hoste S. Kinetics of consecutive reactions in the solid state: thermal decomposition of oxalates. Meas Sci Rev. 2001;1:177–80.
39. Vyazovkin S, Wight CA. Kinetics in solids. Annu Rev Phys Chem. 1997;48:125–49.
40. Khawam A, Flanagan DR. Role of isoconversional methods in varying activation energies of solid-state kinetics: I isothermal kinetic studies. Thermochim Acta. 2005;429:93–102.
41. Khawam A, Flanagan DR. Complementary use of model-free and modelistic methods in the analysis of solid-state kinetics. J Phy Chem B. 2005;109:10073–80.
42. Cai J, Liu R. Kinetic analysis of solid-state reactions: precision of the activation energy obtained from one type of integral methods without neglecting the low temperature end of the temperature integral. Solid state Sci. 2008;10:659–63.
43. Raymond CE, Hein WJPN, Delani N. Kinetic analysis of non-isothermal thermogravimetric analyser results using a new method for the evaluation of the temperature integral and multi-heating rates. Fuel. 2006;85:418–22.
44. Brown ME, Gallagher PK, editors. Handbook of thermal analysis and calorimetry, vol 5: recent advances, techniques and applications. Amsterdam: Elsevier; 2008.
45. Burnham AK, Dinh LN. A comparison of isoconversional and model-fitting approaches to kinetic parameter estimation and application predictions. J Therm Anal Calorim. 2007;89:479–90.
46. Ozawa T. A new method of analyzing thermogravimetric data. Bull Chem Soc Jpn. 1965;38:1881–6.
47. Ozawa T. Kinetic analysis of derivative curves in thermal analysis. J Therm Anal Calorim. 1970;2:301–7.
48. Crissafis K, Paraskevopoulos KM, Bikiaris DN. Thermal degradation kinetics of the biodegradable aliphatic polyester, poly(propylene succinate). Polym Degrad Stab. 2006;91:60–8.
49. Vyazovkin S. Model-free kinetics staying free of multiplying entities without necessity. J Therm Anal Calorim. 2006;83: 45–51.
50. Solymosi F. Structure and stability of salts of halogen oxyacids in the solid phase. London: Wiley; 1977.
51. Prout EG, Tompkins FC. The thermal decomposition of potassium permanganate. Trans Faraday Soc. 1944;40:488–97.
52. Helg U. KJO_3, ein Ferroelektrikum mit nicht umklappbarer, jedoch auslenkbarer Polarisation. Z Kristallogr. 1970;131: 241–77.
53. Salje E. Physikalische Eigenschaften von KJO_3. Z Kristallogr. 1971;134:107–15.
54. Naray-Szabo J, Kalman A. On the structure and polymorphism of potassium iodate, KIO_3. Acta Crystallogr. 1961;14:791–2.
55. Stern KH. High temperature properties and thermal decomposition of inorganic salts with oxy anions. Florida: CRC Press; 2001. p. 240.
56. Philips BR, Taylor O. Thermal decomposition of potassium metaperiodate. J Chem Soc 1963;5583–5590.
57. Muraleedharan K, Kannan MP. Effects of dopants on the isothermal decomposition kinetics of potassium metaperiodate. Thermochim Acta. 2000;359:161–8.
58. Muraleedharan K, Kannan MP, Gangadevi T. Effect of metal oxide additives on the thermal decomposition kinetics of potassium metaperiodate. J Therm Anal Calorim. 2010;100:177–82.
59. Muraleedharan K, Kannan MP, Gangadevi T. Thermal decomposition of potassium metaperiodate doped with trivalent ions. hermochim Acta. 2010;502:24–9.
60. Markovitz MM, Boryta DA. The decomposition kinetics of lithium perchlorate. J Phys Chem. 1961;65:1419–24.
61. Kannan MP, Abdul Mujeeb VM. Effect of dopant ion on the kinetics of thermal decomposition of potassium bromate. React Kinet Catal Lett. 2001;72:245–52.
62. Kim S, Kavitha D, Yu TU, Jung JS, Song JH, Lee SW, Kong SH. Using isothermal kinetic results to estimate kinetic triplet of pyrolysis reaction of polypropylene. J Anal Appl Pyro. 2008; 81:100–5.
63. Huheey JE. Inorganic chemistry principles of structure and reactivity. New York: Harper & Row Publishers; 1983.